Supplementary Information (SI) for

How the sustainable solvent water unleashes the photoredox catalytic potential of ruthenium polypyridyl complexes for pinacol couplings

*By Robert Naumann and Martin Goez**

Contents

*Dr. Robert Naumann, Prof. Dr. Martin Goez,
Martin-Luther-Universität Halle-Wittenberg, Institut für Chemie, Kurt-Mothes-Str. 2, D-06120 Halle (Saale), Germany.
E-mail: martin.goez@chemie.uni-halle.de

1 Materials and methods

RuDmb was synthesized as described previously.[1] All other chemicals were commercially available and used as received. Solutions in aqueous media were prepared with ultrapure Millipore MilliQ water (specific resistance, 18.2 MΩ cm). All studies were carried out with oxygen exclusion, by bubbling argon 5.0 through the solutions for 45 min before the start and maintaining an argon atmosphere above the solutions during the experiments.

All mechanistic investigations on short timescales were performed with a home-made laser flash photolysis setup. A frequency-doubled Nd:YAG laser with a pulse width of *ca.* 5 ns served to excite the solution in the observation cell with a wavelength of 532 nm. To ensure homogeneous excitation, the laser beam was collimated but not focused, and the solutions were kept optically thin by employing sufficiently low concentrations of the ruthenium complexes. Owing to the short optical pathlength in the direction of the beam (0.2 cm), this allowed linearizing the Lambert–Beer law with negligible error. Observation of fluorescence or absorption was done at right angles to the excitation; and for better sensitivity, the pertaining optical path length was 0.4 cm. The linearity of the detection photomultiplier was such that any luminescence artifacts were completely removable from absorption traces by difference experiments. A step-motor driven flow-through system that was activated after each flash ensured that repetitive experiments for improving the signal-to-noise ratio only involved pristine solution.

For preparative illuminations, 35 ml of degassed solution were transferred to a cylindrical cuvette (inner diameter, 4.8 cm; length along the axis, 2 cm) equipped with a cooling mantle on the side facing away from the entrance window. The solution temperature was maintained at 20 °C during irradiation with a UHP-T-LED-460 (460 nm; radiative power, 4.3 W; beam profile, quadratic with 3.2 cm sides; beam direction, parallel to the cuvette axis) for the specified time under vigorous stirring with an inserted bar magnet. The progress of the photoreactions and the end-point yields were determined by ^{1}H-NMR, using aliquots of 2.5 ml and adding to them 10 % (v/v) D_2O for shimming and locking plus a weighed-in amount of solid fumaric acid or 2,2-dimethyl malonic acid as inner standard for the concentrations. The volume change by the repeated removal of aliquots during preparative illumination is taken into account mathematically by a straightforward correction.[2] Because important diagnostic signals are obscured by resonances of SDS or (2-hydroxypropyl)-β-cyclodextrin, the solutions at end-point were also exhaustively extracted with diethyl ether. After evaporating the ether, the residue was taken up in $CDCl_3$, and its ^{1}H-NMR was recorded.

Specific modifications of these experimental details are recorded in the pertaining sections below.

2 Mechanistic details and control experiments

2.1 MLCT quenching in water

2.1.1 Phenolates as quenchers

To determine the rate constants of MLCT quenching, we recorded the luminescence decays at the emission maximum (*ca.* 600 nm) following excitation of RuBpy or RuDmb with a green laser flash (532 nm). At least four different nonzero concentrations of each quencher were used. The ionic strength was adjusted to 0.1 M by adding NaCl.

Supplementary Figure 1 displays an example for each complex. The superimposed fit curves clearly show that all decays obey pure first-order kinetics; the amplitudes directly after the laser flash do not depend on the quencher concentration, hence there is no static quenching; and the Stern–Volmer plots of the observed rate constants are seen to be linear. The same behaviour was observed also with all the other phenolates.

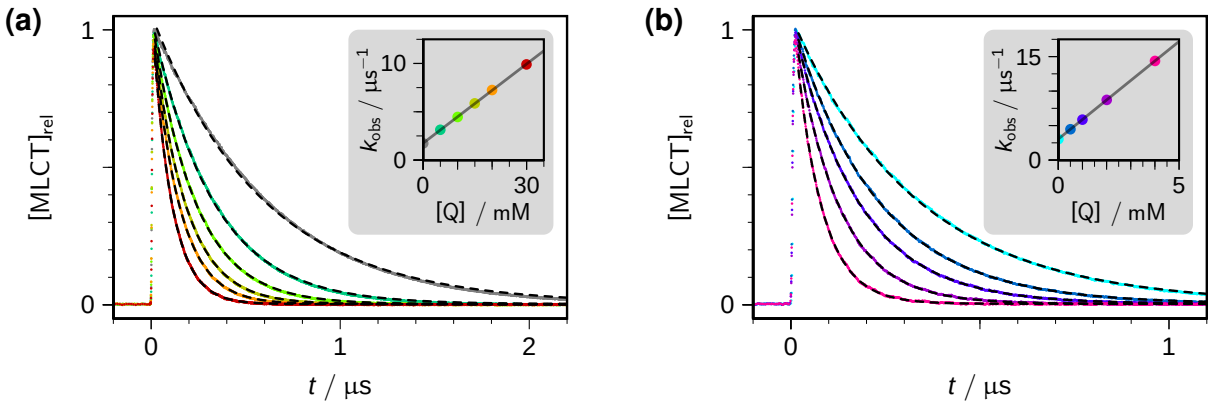

Supplementary Figure 1: Examples of the MLCT quenching experiments by phenolates. Common conditions, 50 µM ruthenium complex in water at pH 12.7 (NaOH) and ionic strength 0.1 M (adjusted with NaCl); excitation with a 532 nm pulse of duration 5 ns and intensity 608 mM cm^{-2}. In each graph, all decay curves have been normalized to the maximum of the unquenched signal, and are overlaid with dashed best-fit curves $\exp(-k_{obs}t)$. The insets display k_{obs} as functions of the concentration of the respective quencher Q, with the same colour code for corresponding curves in the main plot and data points in the inset. The slope of the regression line gives the bimolecular rate constant k_q of the quenching. Graph (a), complex RuBpy with quencher *p*-fluorophenolate, $k_q = 2.72 \times 10^8$ M^{-1}s^{-1}; graph (b), complex RuDmb with quencher *p*-methoxyphenolate, $k_q = 2.81 \times 10^9$ M^{-1}s^{-1}. For further explanation, see the text.

The bimolecular rate constants k_q obtained from the Stern–Volmer plots have been collected in Supplementary Table 1. The main plot of Figure 1 of the main article is based on these data.

Owing to the low polarity of cyclodextrin cavities, the dicationic complexes RuBpy and RuDmb are not complexed by (2-hydroxypropyl)-β-cyclodextrin.[3] In contrast, they do associate with the anionic SDS micelles, as is evidenced by shifts of their absorption and luminescence bands, and the fact that MLCT quenching by Asc^{2-} is slower by two orders of magnitude in aqueous SDS.[1] While the association may have some effect on the standard potential $E^{\ominus}(\mathrm{GS/OER})$, the strong deceleration makes a determination by the same series of phenolates as in Supplementary Table 1 impracticable.

Supplementary Table 1: Phenolate quenchers of this work, their standard potentials $E^{\ominus}$ under our conditions, and obtained rate constants k_q for quenching the MLCT states of the complexes RuBpy and RuDmb

Quencher	$E^{\ominus}$ / V [a]	k_q / $\left(10^8\,M^{-1}s^{-1}\right)$	
		RuBpy	RuDmb
4-NH_2PhO$^-$	0.22	49.7	38.7
2,6-diMeOPhO$^-$	0.42	59.3	47.2
4-MeOPhO$^-$	0.56	49.4	28.1
4-EtPhO$^-$	0.71	19.5	0.63
4-FPhO$^-$	0.78	2.72	0.13
PhO$^-$	0.83	1.83	0.046
4-ClPhO$^-$	0.83	1.86	—
2-ClPhO$^-$	0.93	0.66	—
4-AcPhO$^-$	1.0	0.037	—

[a] Standard potential of the couples RPhO$^{\bullet}$ / RPhO$^-$ employed in this work, from a compilation in the literature.[4]

2.1.2 Rehm–Weller analysis

The empirical Rehm–Weller equation,[5]

$$k_q = \frac{k_d}{1 + \frac{k_{-d}}{Z}\left[\exp\left(\frac{\Delta G^{\ominus}}{RT}\right) + \exp\left(\frac{\Delta G^{\ddagger}}{RT}\right)\right]} \tag{S1}$$

expresses the second-order rate constant k_q of an electron-transfer quenching process with the thermodynamic driving force $\Delta G^{\ominus}$, the activation Gibbs energy $\Delta G^{\ddagger}$, the rates of formation and separation of an encounter complex (k_d and k_{-d}), the universal collision factor Z, the gas constant R and the absolute temperature T. (In the main article, we have specified the energies in multiples of RT, abbreviated k_{-d}/Z as k'_{-d} and also inserted Supplementary Equation S4 below, to simplify the formula.)

$\Delta G^{\ominus}$ is composed of the free energies for oxidizing the donor and reducing the acceptor (standard potentials, $E^{\ominus}_{ox}$ and $E^{\ominus}_{red}$), the free energy of the excited state (E^*; as obtainable from the 0–0 band, *i.e.* the absorption and luminescence spectra), and the work terms w_r and w_p arising from the Coulombic interactions between the species before and after the electron transfer:

$$\Delta G^{\ominus} = E^{\ominus}_{ox} - E^{\ominus}_{red} - E^* + w_p - w_r \tag{S2}$$

The Coulombic terms w_x are

$$w_x = N_A \frac{z_A z_B e^2}{4\pi\varepsilon_0\varepsilon_r d} f \tag{S3}$$

with the charges $z_{A,B}$ on, and reaction distance d between, species A and B; the relative

permittivity ε_r; the shielding factor by the ionic atmosphere, f;[6] and the fundamental constants N_A, e and ε_0. Because the $ArO^\bullet$ are uncharged, w_p equals zero. With the charges on MLCT and ArO^-, +2 and −1, a smallest reaction distance d of 10.9 Å (for RuBpy and unsubstituted phenolate; see below), and a relative permittivity of 80.1 at 20 °C, w_r is calculated to be at most 0.033 eV even at an ionic strength of zero (f = 1); and at the ionic strength of this work, where f equals 0.6 in water,[6] w_r thus amounts to less than 0.02 eV in the worst case. In view of this small size and the other uncertainties involved, we thus regard this work term as negligible.

$\Delta G^\ddagger$ is given by[5]

$$\Delta G^\ddagger = \frac{\Delta G^\ominus}{2} + \sqrt{\left(\frac{\Delta G^\ominus}{2}\right)^2 + \left(\frac{\lambda}{4}\right)^2} \quad \text{(S4)}$$

The reorganization energy λ has an inner and an outer contribution, λ_i and λ_o. The former stems from the changes of the bond lengths. It would require a time-consuming normal-coordinate analysis for strict calculation but is, fortunately, significantly smaller than λ_o: for RuBpy, its is negligible;[7] for phenolates, it was estimated to be around 0.2 eV because of noticeable changes of the carbon–oxygen bond length upon oxidation.[8]

For spherical reactants with diameters d_A and d_B and encounter distance d, λ_o can be calculated with a continuum model,[9]

$$\lambda_o = \frac{N_A e^2}{4\pi\varepsilon_0}\left(\frac{1}{d_A} + \frac{1}{d_B} - \frac{1}{d}\right)\left(\frac{1}{n^2} - \frac{1}{\varepsilon_r}\right) \quad \text{(S5)}$$

where n is the index of refraction. The solvent-dependent term in the second bracket on the r.h.s. of Supplementary Equation S5 equals 0.552 in our case, but uncertainties arise from the geometrical term in the first bracket. While the complexes are well describable as spheres, phenolates possess ellipsoidal shapes; and even though a model exists to describe that complication,[10] the quantity d may well be larger than the distance of closest approach $(d_A + d_B)/2$.[11] As an estimate, the calculated molecular diameters of 14.2 Å (RuBpy) and 7.6 Å (unsubstituted phenolate) and the assumption of closest approach yield an outer reorganization energy of 0.87 eV, and thus a total of 1.07 eV for λ.

The Einstein–Smoluchowski relationship, with the Debye modification for charged reactants,[12] leads to a value of $8.9 \times 10^9\ M^{-1}s^{-1}$ for k_d, which also needs to regarded as approximate. Even larger uncertainties apply to k_{-d}/Z, for which Rehm and Weller took a value of 0.25 in acetonitrile,[5] but Eberson chose 0.1, stating the the fits were rather insensitive to it;[6] and for MLCT quenching by phenolates in water, other authors even assumed values of as low as 0.03.[8]

To scan the parameter space, we carried out a series of fits to the data set of Figure 1 of the main article with k_{-d}/Z fixed at 0.01, 0.05, 0.09, 0.13, or 0.17, and for each of these values allowed the other parameters to vary. With visual indistinguishability except for very small effects in the plateau region, this gave best-fit k_d between $6.4 \times 10^9\ M^{-1}s^{-1}$ and

$7.4 \times 10^9\,\mathrm{M^{-1}s^{-1}}$; and best-fit λ between 0.77 eV and 0.5 eV. Hence, these parameters roughly fall into the expected regions, but none of them can be extracted reliably. However, we found no such variations of the quantity of interest, $\Delta G^{\ominus}$ and thus $E^{\ominus}(\mathrm{GS/OER})$: all fits converged on standard potentials of -1.30 V for RuBpy and -1.41 V for RuDmb, with an uncertainty of not more than ± 0.006 V. In contrast, fixing $\Delta G^{\ominus}$ at the value in acetonitrile shifted the fall-off of the curve in such a way that could not be compensated by a variation of the other parameters.

2.1.3 Control experiments

As control experiments for the interception experiments of the next Section, we first ascertained that the substrates to be transformed by OER do not quench MLCT to a degree that would influence the mechanism. Supplementary Figure 2a illustrates this for benzaldehyde PhCHO and anisaldehyde AnCHO. As is evident from comparing the traces with those of Supplementary Figures 3a and 4a, where $\mathrm{Asc^{2-}}$ quantitatively quenches MLCT to give OER within *ca.* 200 ns, no quenching by the aldehydes alone is discernible on that timescale even at 2.5 to 3 times higher aldehyde concentrations; and only on the timescale of 1 μs, some negligible quenching can be perceived under these conditions, if at all.

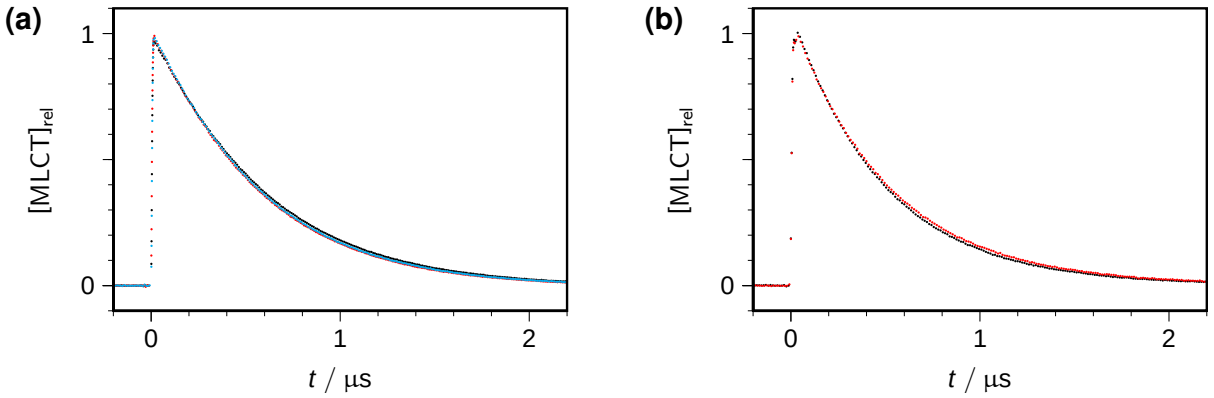

Supplementary Figure 2: Absence of MLCT quenching by aromatic aldehydes or alphatic amines in water. Common conditions, 50 μM RuBpy in water at pH 12.7 (NaOH); excitation with a 532 nm pulse of duration 5 ns and intensity *I*; black data points, without quencher. Graph (a), I = 357 mJ cm^{-1}; unsuccessful quenchers, 10 mM benzaldehyde (cyan) or anisaldehyde (red). Graph (b), I = 375 mJ cm^{-1}; unsuccessful quencher, 200 mM DABCO (red). For further explanation, see the text.

Second, in connection with Section 2.2.2 where we successfully generated OER of RuBpy in acetonitrile by quenching the MLCT state with the aliphatic amine DABCO (diazabicyclo[2.2.2]octane), the control experiment of Supplementary Figure 2b demonstrates that the same approach clearly fails in water: there is no MLCT quenching at all; on the contrary, the MLCT life is slightly lengthened in the presence of 200 mM DABCO, which we ascribe to the scavenging of residual oxygen by the amine. As the MLCT energy is only marginally influenced by the change of solvent, as is evident from the very small effect on the absorption and emission spectra, this control experiment thus corroborates a higher energy of OER in the protic solvent.

2.2 OER interception by substrate

All the experiments in this Section were carried out with RuBpy. We observed OER through its absorption, with the monitoring wavelength set to the isosbestic point of GS and MLCT. This point lies between 500 nm (acetonitrile) and 514 nm (aqueous SDS); and we determined it directly in our laser flash photolysis setup before the start of each series of experiments in a given reaction medium.

2.2.1 Aqueous medium

As opposed to acetonitrile, where no interception by the substrate occurs (see below, Section 2.2.2), a small complication arises in aqueous medium because the radical anion of the substrate also absorbs at the observation wavelength, as is especially noticeable in the case of AnCHO (see, *e.g.*, Supplementary Figure 8a). However, that residual signal decays on a much slower timescale, so we fitted the late part of the curves (at times longer than those displayed in the graphs) with a decreasing linear or an exponential function and subtracted this fit function from the early part. The required back extrapolation is uncritical because the radical anions are very long-lived. In all the traces shown in this Section, the long-term behaviour has been included in the overlaid fit functions; furthermore, all traces have been normalized to the global absorption maximum for each series of experiments, with the corresponding OER concentration specified in the figure captions. This maximum occurs shortly after the laser flash, when no or only very little substrate radical anion is present yet; hence, no uncertainty is involved in determining the OER concentration from the absorption at that point of time.

2.2.1.1 Homogeneous solution

OER is formed through a first-order process but decays with mixed first- and second-order kinetics, the latter due to the recombination with the stoichiometrically formed ascorbyl radicals $\mathrm{Asc}^{\bullet-}$.[13] Although a closed-form analytical solution can be derived for the time dependence of the OER concentration, that solution contains special functions and is very unwieldy.

A much simpler solution can be obtained by waiting until the OER formation has been completed, *i.e.*, by describing only the subsequent decay. When a species with initial concentration c_0 disappears through parallel first- and second-order processes with rate constants k_1 and k_2, its concentration c as function of the time t equals

$$c(t) = \frac{c_0}{\exp[k_1 t](1 + r) - r} \tag{S6}$$

where r is the ratio of initial decay rates,

$$r = \frac{k_2 c_0}{k_1} \tag{S7}$$

After taking into account the long-term behaviour as described above, we fitted the subtraction result with Supplementary Equation S6, using the trace without substrate to determine the start of the fit interval (see, *e.g.*, the dashed superimposed fit curves in Supplementary Figure 3a) and the value of k_2. The concentration c_0 at the fit start follows from the extinction at that point of time.

Supplementary Figures 3 and 4 collect the results for PhCHO and AnCHO in water. The extracted first-order rate constants k_1 are seen to be proportional to the aldehyde concentrations; and the factor of about 6 between the bimolecular rate constants obtained from the proportionality constants, $3.7 \times 10^9\ \mathrm{M^{-1}s^{-1}}$ for PhCHO and $6.0 \times 10^8\ \mathrm{M^{-1}s^{-1}}$ for AnCHO, is consistent with expectation that the more electron-rich substrate AnCHO should be more difficult to reduce.

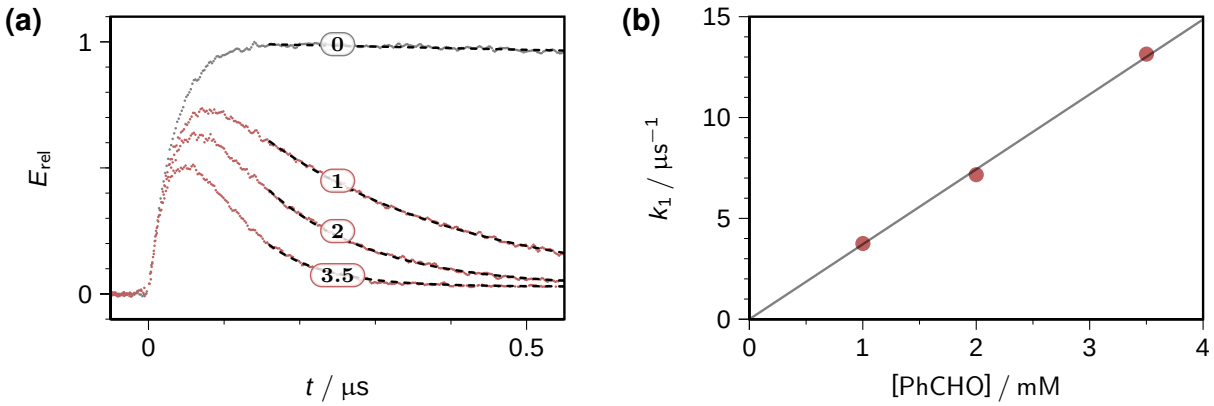

Supplementary Figure 3: Intercepting OER of RuBpy by benzaldehyde PhCHO in homogeneous aqueous solution. Conditions, 50 µM RuBpy and 5 mM Asc^{2-} in water at pH 12.7 (NaOH); OER generation with a 532 nm laser pulse (5 ns, 389 mJ cm^{-2}). Graph (a), traces with the PhCHO concentrations (in mM) given as labels on the curves; all curves normalized to the maximum extinction without PhCHO, corresponding to an OER concentration of 15.8 µM; overlaid black dashed fit curves, $c_0/\,(1 + k_2 c_0 t)$ for the measurement without PhCHO and Supplementary Equation S6 (with correction for the absorption of the PhCHO radical anion) for the others, all in the fit interval used. Graph (b), k_1 as function of the PhCHO concentration, with the slope of the regression line through the origin giving a bimolecular rate constant of $3.6 \times 10^9\ \mathrm{M^{-1}s^{-1}}$. For further explanation, see the text.

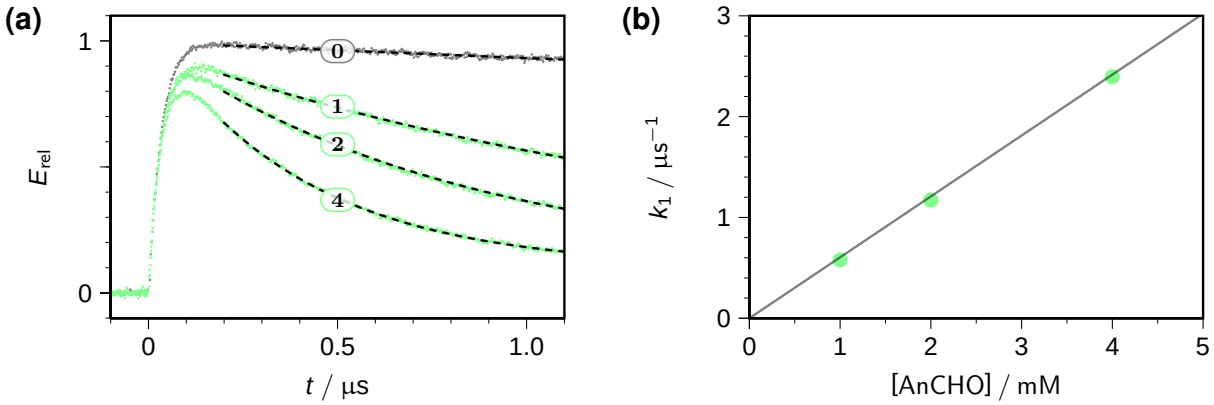

Supplementary Figure 4: Intercepting OER of RuBpy by anisaldehyde AnCHO in homogeneous aqueous solution. Conditions, 50 µM RuBpy and 5 mM Asc^{2-} in water at pH 12.7 (NaOH); OER generation with a 532 nm laser pulse (5 ns, 398 mJ cm^{-2}). Graph (a), traces with the AnCHO concentrations (in mM) given as labels on the curves; all curves normalized to the maximum extinction without AnCHO, corresponding to an OER concentration of 16.1 µM; overlaid black dashed fit curves, $c_0/\,(1 + k_2 c_0 t)$ for the measurement without AnCHO and Supplementary Equation S6 (with correction for the absorption of the AnCHO radical anion) for the others, all in the fit interval used. Graph (b), k_1 as function of the AnCHO concentration, with the slope of the regression line through the origin giving a bimolecular rate constant of $6.0 \times 10^8\ \mathrm{M^{-1}s^{-1}}$. For further explanation, see the text.

2.2.1.2 SDS micelles

RuBpy predominantly resides in the micellar Stern layer,[14] and substrates will partition between the aqueous bulk and the SDS micelles depending on their hydrophobicity, so that interception of OER can occur both across the micelle–water boundary and intramicellar. The former is a simple pseudo first-order process, but the kinetics of the latter is further complicated by the Poisson statistics of micellar occupation.[15]

Although the integrated rate law for the homogeneous case is thus unlikely to provide a correct description of the interception in micellar systems, it can nevertheless be used as a fit function over a limited time interval to extract the initial slopes and analyse their dependence on the substrate concentration. Supplementary Figures 5 and 6 illustrates that this approach is viable for PhCHO and AnCHO in aqueous SDS micelles, and yields apparent rate constants k_1 that are proportional to the substrate concentration.

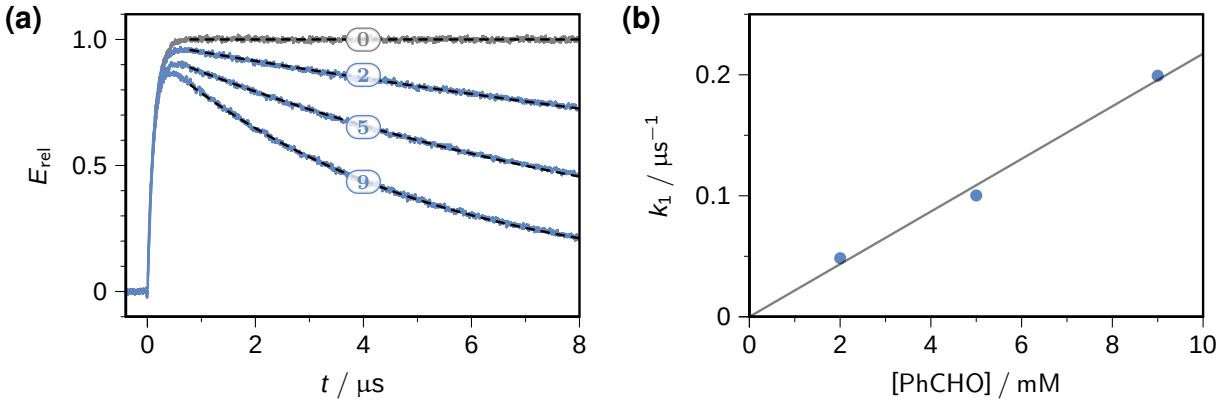

Supplementary Figure 5: Intercepting OER of RuBpy by benzaldehyde PhCHO in a micellar system. Conditions, 50 μM RuBpy and 100 mM Asc^{2-} in 50 mM aqueous SDS at pH 12.7 (NaOH); OER generation with a 532 nm laser pulse (5 ns, 366 mJ cm^{-2}). Graph (a), traces with the PhCHO concentrations (in mM) given as labels on the curves; all curves normalized to the maximum extinction without PhCHO, corresponding to an OER concentration of 20.8 μM; overlaid black dashed fit curves, $c_0/(1 + k_2 c_0 t)$ for the measurement without PhCHO and Supplementary Equation S6 (with correction for the absorption of the PhCHO radical anion) for the others, all in the fit interval used. Graph (b), apparent k_1 as function of the PhCHO concentration, with the slope of the regression line through the origin giving a bimolecular rate constant of 2.2×10^7 M^{-1}s^{-1}. For further explanation, see the text.

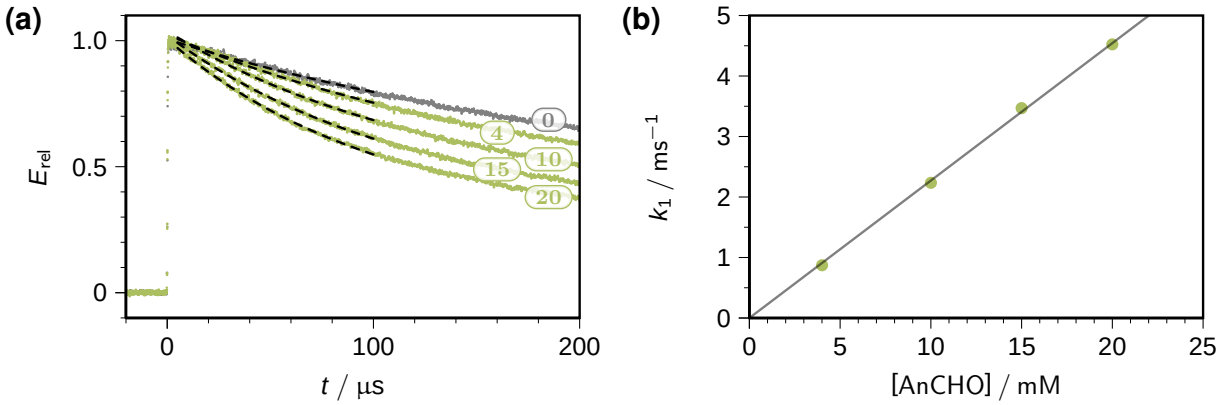

Supplementary Figure 6: Intercepting OER of RuBpy by anisaldehyde AnCHO in a micellar system. Conditions, 50 μM RuBpy and 100 mM Asc^{2-} in 50 mM aqueous SDS at pH 12.7 (NaOH); OER generation with a 532 nm laser pulse (5 ns, 357 mJ cm^{-2}). Graph (a), traces with the AnCHO concentrations (in mM) given as labels on the curves; all curves normalized to the maximum extinction without AnCHO, corresponding to an OER concentration of 20.4 μM; overlaid black dashed fit curves, $c_0/(1 + k_2 c_0 t)$ for the measurement without AnCHO and Supplementary Equation S6 (with correction for the absorption of the AnCHO radical anion) for the others, all in the fit interval used. Graph (b), apparent k_1 as function of the AnCHO concentration, with the slope of the regression line through the origin giving a bimolecular rate constant of 2.3×10^5 M^{-1}s^{-1}. For further explanation, see the text.

As expected, the same reactivity order, PhCHO $>$ AnCHO, as in homogeneous solution is found, but the bimolecular rate constants of the interception differ much more strongly, by a factor of 100 ($2.2 \times 10^7\,M^{-1}s^{-1}$ for PhCHO and $2.3 \times 10^5\,M^{-1}s^{-1}$ for AnCHO), which may well reflect a lower reducing power of OER in the less polar surroundings. The greatly reduced rate constants compared to those in the homogeneous medium would disfavour SDS, were they not compensated by a greatly increased intrinsic stability of OER.[13] As is obvious from Supplementary Figure 6a, in the absence of a substrate OER easily persists for milliseconds because its only decay pathway is the bimolecular recombination with the stoichiometrically formed ascorbyl radical $Asc^{\bullet-}$, which the Coulombic repulsion by the anionic micelle decelerates even more strongly.

2.2.1.3 Cyclodextrin

RuBpy is not known to — and on account of its charge also not expected to — associate with cyclodextrins.[3] This is corroborated by unchanged absorption and luminescence spectra of RuBpy when (2-hydroxypropyl)-β-cyclodextrin HPCD is added.

The less polar substrates will distribute between the cyclodextrin interior and the aqueous bulk. Let K be the equilibrium constant for the association of the substrate S by the cyclodextrin C to give the complex S@C,

$$K = \frac{[S@C]}{[S]\,[C]} \tag{S8}$$

and denote the weight-in concentrations as s_0 and c_0. Because aldehydes such as PhCHO or AnCHO form 1:1 complexes with HPCD,[16] the mass balance is

$$s_0 = [S] + [S@C] \tag{S9a}$$

$$c_0 = [C] + [S@C] \tag{S9b}$$

and the equilibrium concentration of free substrate is

$$[S] = \frac{\sqrt{[1 - (c_0 - s_0)\,K]^2 + 4c_0K} - [1 + (c_0 - s_0)\,K]}{2K} \tag{S10}$$

(The other solution of the underlying quadratic equation yields nonphysical, *i.e.* negative, concentrations.)

With the rate constants k_{free} and $k_{complexed}$ for the reaction of OER with S and S@C, the observed rate constant k_{obs} is

$$\begin{aligned} k_{obs} &= k_{free} \cdot [S] + k_{complexed} \cdot [S@C] \\ &= \left(k_{free} - k_{complexed}\right) \cdot [S] + k_{complexed} \cdot s_0 \end{aligned} \tag{S11}$$

The clearest picture is obtained by varying the cyclodextrin concentration at constant

substrate concentration: because the reaction across the cyclodextrin–water interface cannot be faster than that in the aqueous bulk, k_{obs} is expected to decrease with increasing c_0. Supplementary Figures 7 and 8 display the results for benzaldehyde and anisaldehyde.

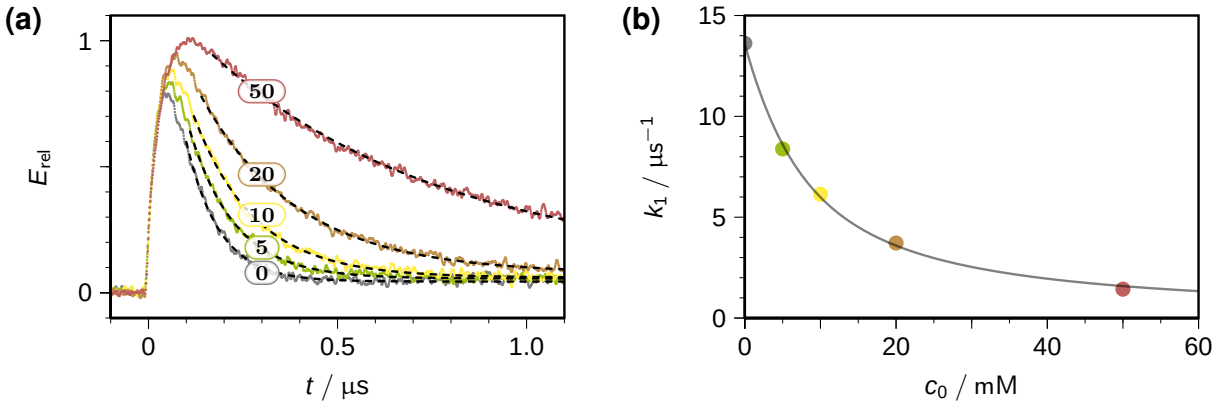

Supplementary Figure 7: Intercepting OER (bpy) by 4 mM benzaldehyde PhCHO in aqueous (2-hydroxypropyl)-β-cyclodextrin. Conditions, 50 µM RuBpy and 5 mM Asc^{2-} in water at pH 12.7 (NaOH); OER generation with a 532 nm laser pulse (5 ns, 357 mJ cm^{-2}); identical colour code for the aldehyde concentrations in both graphs. Graph (a), traces with the cyclodextrin weight-in concentrations c_0 (in mM) given as labels on the curves; all curves normalized to the maximum extinction without cyclodextrin, corresponding to an OER concentration of 10.6 µM; overlaid black dashed fit curves, Supplementary Equation S6 (with correction for the absorption of the PhCHO radical anion) in the fit interval used. Graph (b), observed rate constants k_1 for the interception of OER by PhCHO as functions of c_0; overlaid solid curve, fit of Supplementary Equations S10–S11 to the data; best-fit values, K = 160 M^{-1}, k_{free} = 3.5 × 10^9 M^{-1}s^{-1}, $k_{complexed} \approx 0$. For further explanation, see the text.

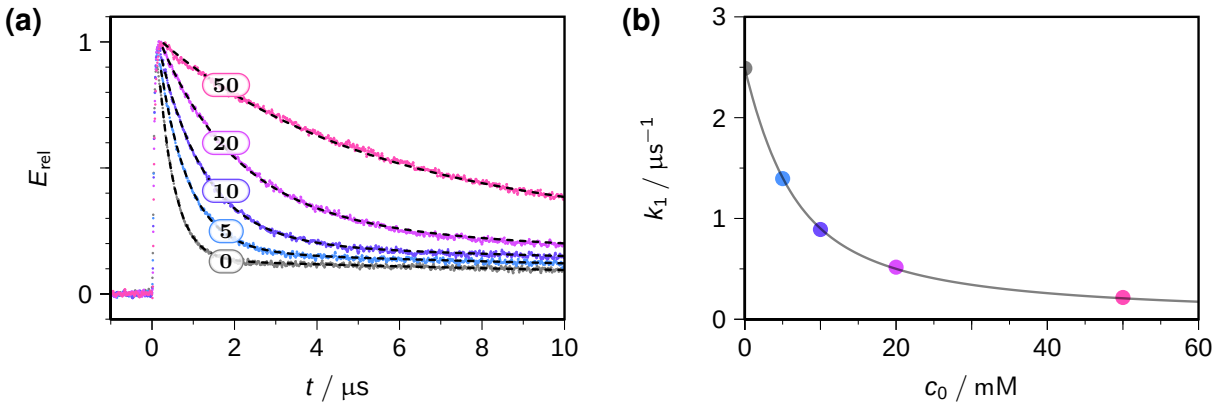

Supplementary Figure 8: Intercepting OER (bpy) by 4 mM anisaldehyde AnCHO in aqueous (2-hydroxypropyl)-β-cyclodextrin. Conditions, 50 µM RuBpy and 5 mM Asc^{2-} in water at pH 12.7 (NaOH); OER generation with a 532 nm laser pulse (5 ns, 357 mJ cm^{-2}); identical colour code for the aldehyde concentrations in both graphs. Graph (a), traces with the cyclodextrin weight-in concentrations c_0 (in mM) given as labels on the curves; all curves normalized to the maximum extinction without cyclodextrin, corresponding to an OER concentration of 14.0 µM; overlaid black dashed fit curves, Supplementary Equation S6 (with correction for the absorption of the AnCHO radical anion) in the fit interval used. Graph (b), observed rate constants k_1 for the interception of OER by AnCHO as functions of c_0; overlaid solid curve, fit of Supplementary Equations S10–S11 to the data; best-fit values, K = 240 M^{-1}, k_{free} = 6.0 × 10^8 M^{-1}s^{-1}, $k_{complexed} \approx 0$. For further explanation, see the text.

For the fits of the traces (Supplementary Figures 7a and 8a) with Supplementary Equation S6, we determined k_2 separately in the same medium but without aldehyde (curves not shown). The values in the presence of the cyclodextrin were very similar to those in water.

With both aldehydes, the fits of Supplementary Equations S10–S11 converged on very small values of $k_{complexed}$. Following the principle of Occam's razor, we take this to indicate that only the small equilibrium concentrations of the substrates in the aqueous phase are

effective in intercepting OER. The bimolecular rate constants k_{free} are the same as in water, as they should be; and the binding constants K (160 M^{-1} for PhCHO and 240 M^{-1} for AnCHO) reflect the different lipophilicities of the two aldehydes.

2.2.2 Acetonitrile

As the control experiment of Supplementary Figure 9 unambiguously demonstrates, in acetonitrile OER of RuBpy is accessible by quenching MLCT with the amine DABCO — as opposed to in water, compare Section 2.1.3 — but once generated is not intercepted even by the benzaldehyde (in direct contrast to Supplementary Figure 3), let alone by the less reactive anisaldehyde. On the contrary, the OER life is even seen to be slightly lengthened by of the addition of 10 mM benzaldehyde, which might reflect the higher scavenging capacity of the system towards residual oxygen.

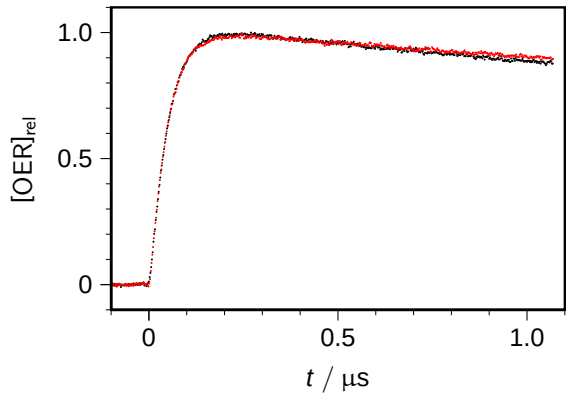

Supplementary Figure 9: Unsuccessful OER interception by benzaldehyde PhCHO in acetonitrile. Conditions, 50 μM RuBpy and 100 mM DABCO; OER generation with a 532 nm laser pulse (5 ns, 352 mJ cm^{-2}). Black and red data points, without PhCHO and with 10 mM PhCHO; both curves normalized to the maximum OER concentration without PhCHO (28.2 μM). For further explanation, see the text.

2.3 Intensity dependence of product formation rate

Under conditions of preparative (*i.e.*, continuous low-intensity) illumination with an LED, the product formation rate is proportional to the LED power P for a monophotonic process, and to $P^{3/2}$ when two photons are pooled with OER as the intermediate.[13] Because the system composition is precisely known only at the start of the illumination, the initial rate v_{init} is the most reliable observable. To rule out that the syntheses of this work involve hydrated electrons $e_{aq}^{\bullet-}$ generated through the pooling mechanism, we determined the photonicity by carrying out the reactions under exactly the same conditions as in Schemes 1–2 of the main article except for variable LED power, stopping the illuminations after 5, 10, and 15 min, and determining the pinacol yields by NMR analysis. The inital product formation rate was obtained by fitting a saturation curve $c_0\,(1 - \exp[-\kappa t])$ to the data, and analytically taking the derivative at $t = 0$ (*i.e.*, $c_0 \times \kappa$).

Supplementary Figure 10 displays the outcome for benzaldehyde and anisaldehyde. Regardless of the substrate, the dependences are clearly linear, in particular in aqueous SDS, which is conducive to the pooling mechanism when the LED intensity is concentrated to a small spot.[1,13] However, the reason why only the monophotonic mechanism operates in the present work is not only the use of the much larger natural beam width but above all the fact that the second step of the pooling mechanism has a quantum yield of not more than a few percent: hence, whenever OER by itself is capable of reducing the substrate, the pathway via photon pooling to give an intermediate of extreme reducing power such as $e_{aq}^{\bullet -}$ is no longer competitive.

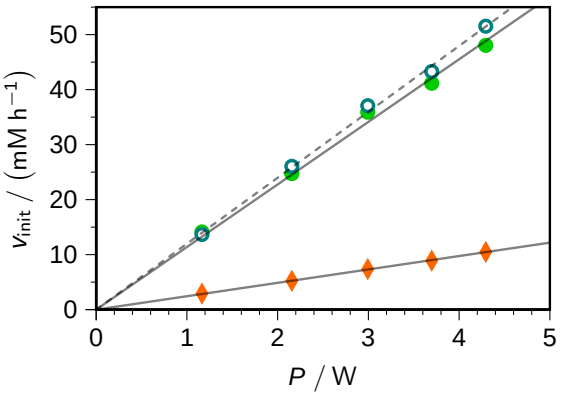

Supplementary Figure 10: Intensity dependences of the initial rate v_{init} of pinacol formation. Conditions, 100 μM RuBpy, 100 mM Asc^{2-}, and 10 mM benzaldehyde (green or teal circles) or anisaldehyde (orange diamonds) in homogeneous aqueous solution (open symbols and broken fit line) or 50 mM aqueous SDS (filled symbols and solid fit line), all at pH 12.7 (NaOH); preparative illumination with a blue LED (460 nm, power P). For further explanation, see the text.

3 NMR spectra of the pinacol coupling products

The colour code in all the spectra of this Section is pinacol, green; benzylic alcohol, orange; residual starting material, magenta. Resonances of unassigned products and of the solvent are displayed in black.

Unless mentioned explicitly in the captions, all displayed extract spectra pertain to the transformations in the aqueous systems without SDS micelles or HPCD as carriers, because the extracts of the carrier systems gave no new information. The relative intensities of the different products in corresponding spectra without and with extraction are not directly comparable owing to the partition coefficients not necessarily being identical.

In the spectra before extraction, only the aromatic regions are displayed because the solvent suppression and the large resonances of the carriers obscure the other ranges.

The catalyst was RuBpy in most cases. However, for comparing the coupling results with AnCHO in the different media (Supplementary Figures 11–15), RuDmb was used because that catalyst gave practically quantitative consumption of the starting materials under all circumstances.

Supplementary Figures 11–13 demonstrate the strong influences of the medium on the chemical shifts and spectral habits of the pinacols, using AnCHO as example.

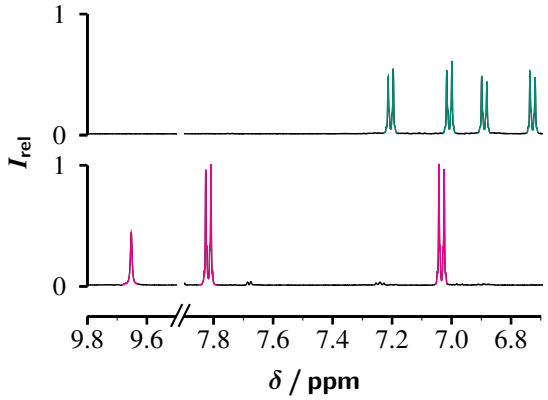

Supplementary Figure 11: NMR spectra of the reaction solution in aqueous base before (bottom) and after (top) the pinacol coupling of anisaldehyde under the conditions of Scheme 1 of the main article. For further explanation, see the text.

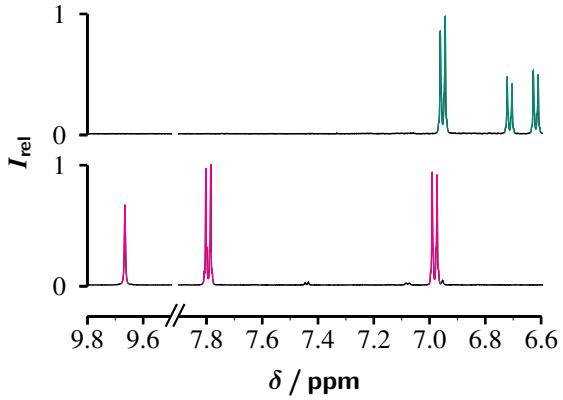

Supplementary Figure 12: NMR spectra of the reaction solution in aqueous SDS before (bottom) and after (top) the pinacol coupling of anisaldehyde under the conditions of Scheme 1 of the main article. For further explanation, see the text.

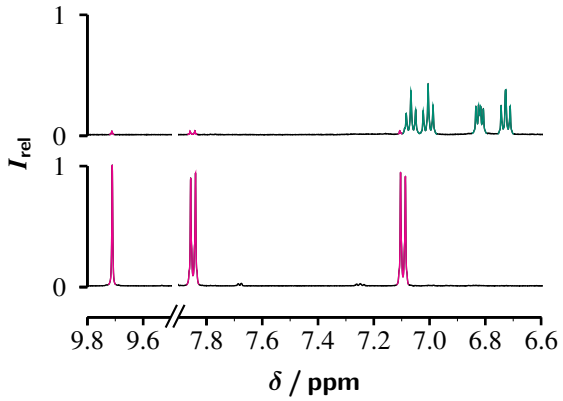

Supplementary Figure 13: NMR spectra of the reaction solution in aqueous (2-hydroxypropyl)-β-cyclodextrin before (bottom) and after (top) the pinacol coupling of anisaldehyde under the conditions of Scheme 1 of the main article. For further explanation, see the text.

Supplementary Figures 14–15 juxtapose the extract spectra from coupling AnCHO of in basic and neutral solution, and illustrate the higher yield of the benzylic alcohol in the latter case; and Supplementary Figures 16–17 serve the same purpose for the substrate PhCHO.

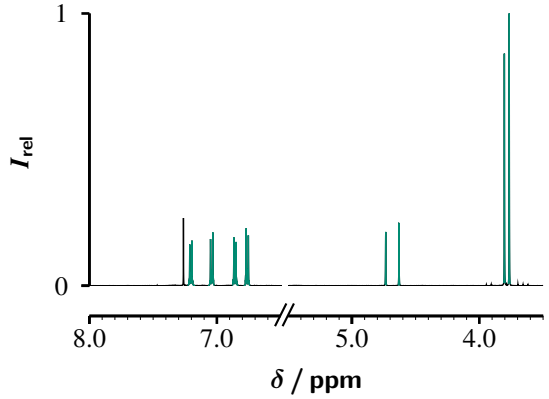

Supplementary Figure 14: NMR spectrum of the extract in the pinacol coupling of anisaldehyde under the conditions of Scheme 1 of the main article (basic solution). For further explanation, see the text.

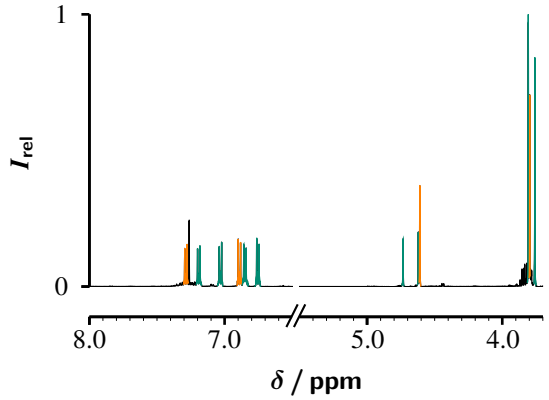

Supplementary Figure 15: NMR spectrum of the extract in the pinacol coupling of anisaldehyde under the conditions of Scheme 2 of the main article (neutral solution). For further explanation, see the text.

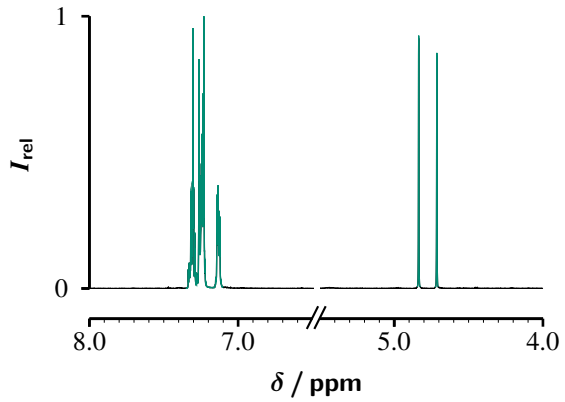

Supplementary Figure 16: NMR spectrum of the extract in the pinacol coupling of benzaldehyde under the conditions of Scheme 1 of the main article (basic solution). For further explanation, see the text.

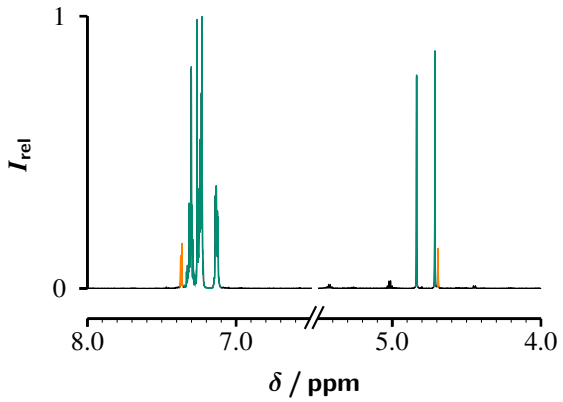

Supplementary Figure 17: NMR spectrum of the extract in the pinacol coupling of benzaldehyde under the conditions of Scheme 2 of the main article (neutral solution). For further explanation, see the text.

Supplementary Figure 18 displays the extract spectrum from the reaction of the water-insoluble 4-chlorobenzaldehyde with HPCD as carrier.

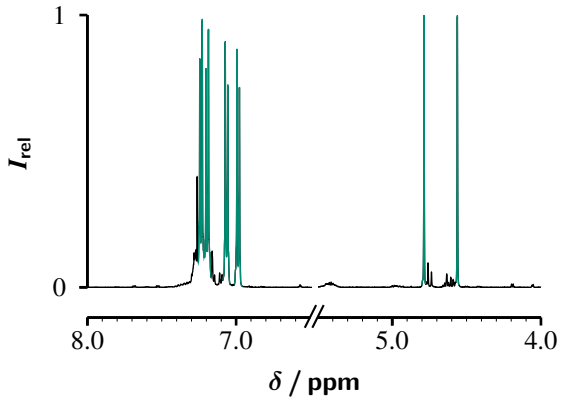

Supplementary Figure 18: NMR spectrum of the extract in the pinacol coupling of 4-chlorobenzaldehyde under the conditions of Scheme 1 of the main article (basic solution with HPCD as carrier). For further explanation, see the text.

The extract spectra of acetophenone, Supplementary Figures 19–20, again show the higher amount of the benzylic alcohol (and the less complete substrate consumption) in neutral solution.

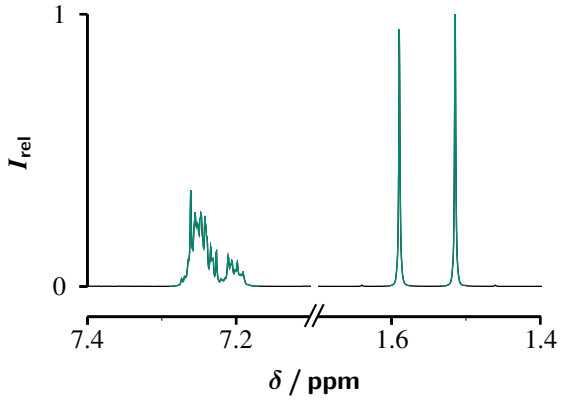

Supplementary Figure 19: NMR spectrum of the extract in the pinacol coupling of acetophenone under the conditions of Scheme 1 of the main article (basic solution). For further explanation, see the text.

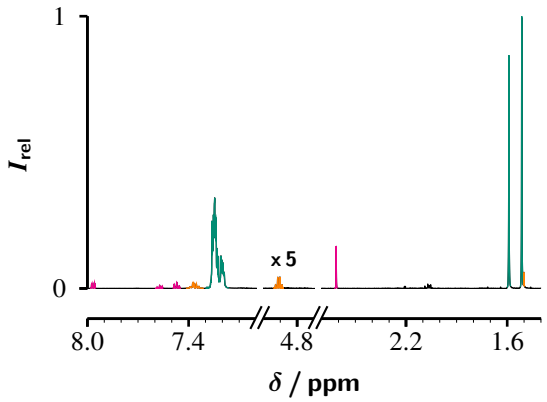

Supplementary Figure 20: NMR spectrum of the extract in the pinacol coupling of acetophenone under the conditions of Scheme 2 of the main article (neutral solution). For further explanation, see the text.

Benzophenone represents a special case because the pinacol precipitates even from the micellar solution. For that reason, the spectrum of the reaction mixture (Supplementary Figure 21) does not contain any pinacol resonances; and dissolving the precipitate yields the pure pinacol spectrum of Supplementary Figure 22.

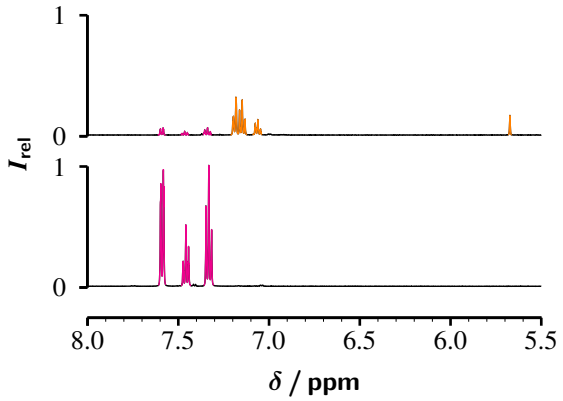

Supplementary Figure 21: NMR spectra of the reaction solution in aqueous SDS before (bottom) and after (top) the pinacol coupling of benzophenone under the conditions of Scheme 1 of the main article. The precipitated pinacol product was removed by filtration before recording the product spectrum. For further explanation, see the text.

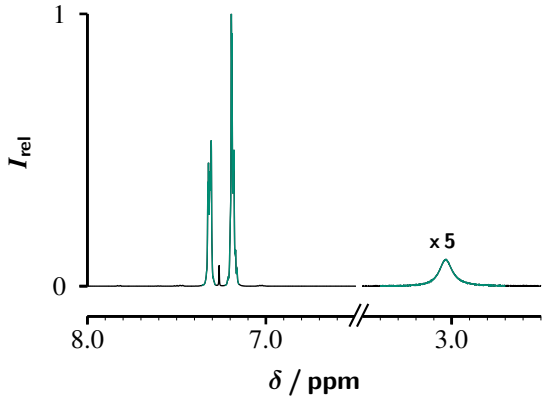

Supplementary Figure 22: NMR spectrum of the precipitated pinacol product in the coupling of benzophenone under the conditions of Scheme 1 of the main article (aqueous SDS). For further explanation, see the text.

The prominent singlet at 7.2 ppm in the extract spectra after coupling furfural, Supplementary Figures 23–24, is due to residual $CHCl_3$ in the deuterated solvent.

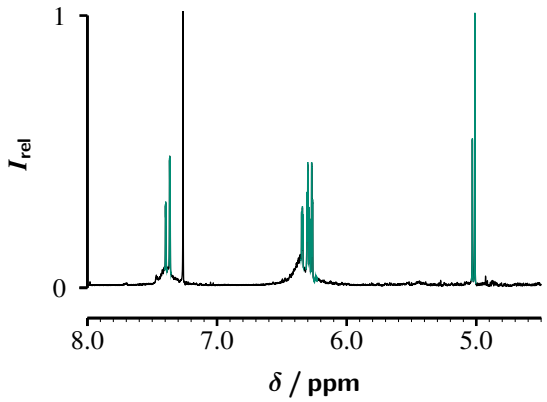

Supplementary Figure 23: NMR spectrum of the extract in the pinacol coupling of furfural under the conditions of Scheme 1 of the main article (basic solution). For further explanation, see the text.

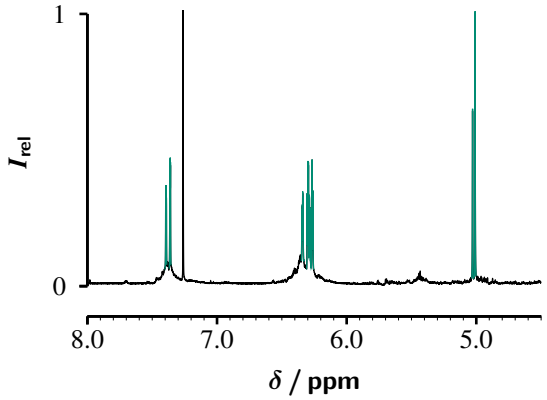

Supplementary Figure 24: NMR spectrum of the extract in the pinacol coupling of furfural under the conditions of Scheme 2 of the main article (neutral solution). For further explanation, see the text.

4 Other reaction types

Supplementary Table 2 contains other types of photoredox catalytic reactions that RuBpy can effect in water owing to the boost of its reducing power. It was possible to carry out all these transformations without adding SDS or cyclodextrins because the starting materials are much more soluble in water than the pinacol precursors were. For the same reason, we were able to double the substrate concentrations while keeping the illumination intensity, wavelength, and duration the same as before.

The general colour code in the ^{1}H-NMR spectra is in analogy to that of the preceding Section, namely, magenta for (residual) starting material, green for the product given in Supplementary Table 2, and black for unassigned minor side products. Deviations from or additions to this colour code are specified in the respective figure captions.

The integrity of the pyridyl moiety is preserved in the hydrogenation of the olefinic double bond of 3- or 4-pyridylacrylate with the water-based RuBpy photoredox catalytic system. The

Supplementary Table 2: Further applications of water-based photoredox catalysis with RuBpy [a]

Reaction type	Substrate	Product	Yield [b]
olefin hydrogenation	3-pyridylacrylate	3-(3-pyridyl)-propionate	73 % (97 %)
olefin hydrogenation	4-pyridylacrylate	3-(4-pyridyl)-propionate	91 % (100 %)
dechlorination	dichloroacetate	chloroacetate	84 % (86 %)
dechlorination	trichloroacetate	chloroacetate [c]	65 % (100 %)
cross coupling [d]	2-chloropyrazine	*N*-methyl-2-(2-pyrazinyl)-pyrrole	45 % (60 %)

[a] Reaction conditions as in Scheme 1 of the main article (0.1 mM RuBpy and 100 mM Asc^{2-} in water at pH 12.7; LED-illumination with 4.3 W @ 460 nm for 3 h) but substrate concentration doubled to 20 mM. [b] Prior to workup; substrate consumption given in parentheses. [c] Side product, 35 % dichloroacetate; 1.6 equivalents of Cl^- liberated from the starting material. [d] Asc^{2-} replaced by 50 mM urate; trapping component, 100 mM *N*-methylpyrrole.

hydrogen donor is the monoanion $HAsc^-$, whose concentration still amounts to a tenth of the ascorbate weight-in concentration at the pH of our experiments.[1] The transformation of 3-pyridylacrylate affords some side products whereas that of 4-pyridylacrylate is essentially clean (Supplementary Figures 25 and 26).

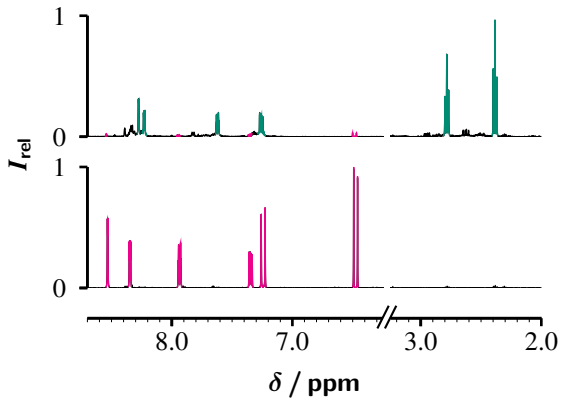

Supplementary Figure 25: NMR spectra of the reaction solution in aqueous base before (bottom) and after (top) the selective hydrogenation of the olefinic bond in 3-pyridylacrylate under the conditions of Supplementary Table 2. For further explanation, see the text.

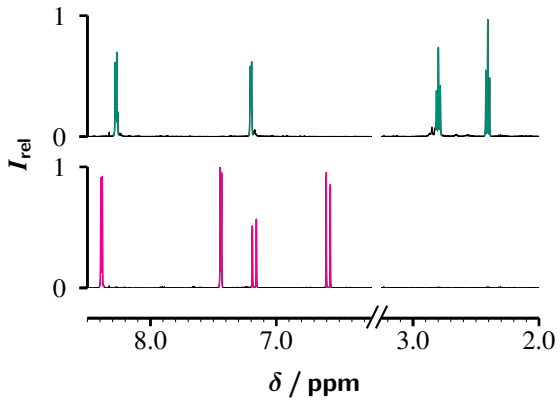

Supplementary Figure 26: NMR spectra of the reaction solution in aqueous base before (bottom) and after (top) the selective hydrogenation of the olefinic bond in 4-pyridylacrylate under the conditions of Supplementary Table 2. For further explanation, see the text.

The dechlorination yields of Supplementary Table 2 were determined by measuring the concentrations of liberated chloride with an ion-sensitive electrode (Hanna Instruments, HI4107) following the manufacturer's protocol. The process unavoidably stops at the stage of chloroacetate because that compound can only be attacked by ultrastrong reductants such as $e_{aq}^{\bullet -}$, which require photon pooling for their generation.[1] Dichloroacetate affords chloroacetate without side reactions (Supplementary Figure 27), as the identical yields of the monochlorinated end product and of Cl^- indicate. The dechlorination of trichloroacetate is also not accompanied by appreciable dimerization, but under our conditions not more than 1.6 equivalents of Cl^- could be liberated before the photoredox catalytic system was exhausted, with the organic products partitioning between mono- and dichloroacetate in a ratio of about 1:2 (Supplementary Figure 28). We stress that the turnover number of 360 in this example, before optimization of conditions, still is gratifyingly high.

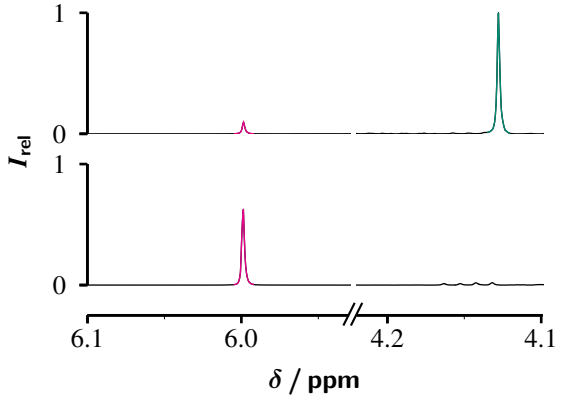

Supplementary Figure 27: NMR spectra of the reaction solution in aqueous base before (bottom) and after (top) the dechlorination of dichloroacetate under the conditions of Supplementary Table 2. For further explanation, see the text.

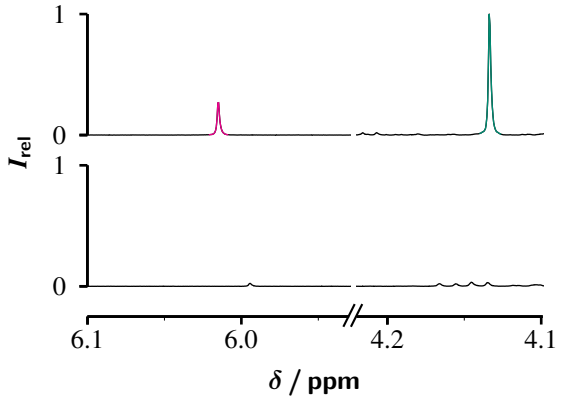

Supplementary Figure 28: NMR spectra of the reaction solution in aqueous base before (bottom) and after (top) the dechlorination of trichloroacetate under the conditions of Supplementary Table 2. The green signal in the product spectrum is dichloroacetate. For further explanation, see the text.

For the dechlorination-induced cross coupling of 2-chloropyrazine, the sacrificial donor ascorbate had to be replaced by urate in order to minimize the exchange of halogen by hydrogen. The pK_a of the hydrogen-donating monoanion is about two units lower in the urate case compared to $HAsc^-$; hence, at the pH of our experiments, the concentration of the hydrogen donor is about two orders of magnitude lower with urate.[17] Being an inexpensive bioavailable and nontoxic compound, urate is an equally sustainable sacrificial donor as is ascorbate.

Without a trapping reagent, the pyrazinyl radicals formed by the RuBpy-induced dechlorination attack their parent compound to give a complex mixture of products, but when a sufficient concentration of *N*-methylpyrrole is added, cross coupling to the 2-position of the pyrrole predominates (Supplementary Figure 29).

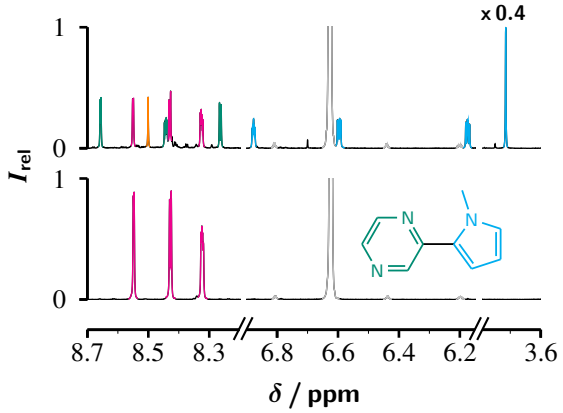

Supplementary Figure 29: NMR spectra of the reaction solution in aqueous base before (bottom) and after (top) the cross coupling of 2-chloropyrazine with *N*-methylpyrrole under the conditions of Supplementary Table 2. The two moieties in the coupling product are displayed in green and cyan (see, formula between the traces); and the orange signal in the product spectrum is due to the dechlorination product pyrazine. The gray signals in both spectra belong to the trapping component *N*-methylpyrrole. For further explanation, see the text.

The examples of this Section demonstrate the broad applicability of the water-based RuBpy photoredox catalytic method.

Supplementary References

[1] R. Naumann, F. Lehmann and M. Goez, *Chem. Eur. J.*, 2018, **24**, 13259–13269.

[2] T. Kohlmann, R. Naumann, C. Kerzig and M. Goez, *Photochem. Photobiol. Sci.*, 2017, **16**, 1613–1622.

[3] J. W. Park, in *Cyclodextrin Materials Photochemistry, Photophysics and Photobiology*, ed. A. Douhal, Elsevier: Amsterdam, 2006, ch. Fluorescence Methods for Studies of Cyclodextrin Inclusion Complexation and Excitation Transfer in Cyclodextrin Complexes, pp. 1–26.

[4] W. A. Arnold, Y. Oueis, M. OConnor, J. E. Rinaman, M. G. Taggart, R. E. McCarthy, K. A. Foster and D. E. Latch, *Environ. Sci. Process. Impacts*, 2017, **19**, 324–338.

[5] D. Rehm and A. Weller, *Isr. J. Chem.*, 1970, **8**, 259–271.

[6] L. Eberson, *Electron transfer reactions in organic chemistry*, Springer-Verlag, Berlin, 1982.

[7] M. Venturi, Q. G. Mulazzani, M. D'Angelantonio, M. Ciano and M. Z. Hoffman, *Radiat. Phys. Chem.*, 1991, **37**, 449–456.

[8] P. Thanasekaran, S. Rajagopal and C. Srinivasan, *J. Chem. Soc., Faraday Trans.*, 1998, **94**, 3339–3344.

[9] R. A. Marcus, *Annu. Rev. Phys. Chem.*, 1964, **15**, 155–196.

[10] M. E. Peover and J. S. Powell, *J. Electroanal. Chem.*, 1969, **20**, 427–433.

[11] M. Goez, *Z. Phys. Chem. (Muenchen, Ger.)*, 1990, **169**, 133–145.

[12] P. Debye, *Trans. Electrochem. Soc.*, 1942, **82**, 265.

[13] R. Naumann, F. Lehmann and M. Goez, *Angew. Chem. Int. Ed.*, 2018, **57**, 1078–1081.

[14] C. Kerzig and M. Goez, *Chem. Sci.*, 2016, **7**, 3862–3868.

[15] T. Kohlmann, R. Naumann, C. Kerzig and M. Goez, *Phys. Chem. Chem. Phys.*, 2017, **19**, 8735–8741.

[16] B. A. Demian, *Carbohyd. Res.*, 2000, **328**, 635–639.

[17] R. Naumann and M. Goez, *Chem. Eur. J.*, 2018, **24**, 9833–9840.